Supercritical Flow Effects on Some Unsteady Aerodynamic Coefficients Used for Flutter Analysis

JEROME E. FISCHLER*
McDonnell Douglas Corporation, Long Beach, Calif.

The unsteady acrodynamic derivative changes due to shock and flow separation have been examined in detail. Unconservative results can be obtained for flutter if the supercritical pressure distribution effects are not accounted for. Theoretical, wind-tunnel, and flight-test results of the derivatives and the resulting flutter speeds are compared. The considerations to obtain a more realistic representation of the aerodynamics used in harmonic and transient analysis are discussed and illustrated. Examples of two- and three-dimensional effects of supercritical unsteady aerodynamics are shown. If care is taken to represent the unsteady derivatives with the proper phase angle and magnitude along the wing correcting for the depth of penetration into the supercritical regime, the predicted results will compare relatively well with the flight test results. Much of the work in this paper discusses the method by which real and imaginary terms, representing compressibility, the vertical force coefficient due to angle of attack, and aileron hinge moment, were modified to represent the experimental data available at supercritical speeds.

Introduction

PRESENT-DAY subsonic aircraft fly in the supercritical speed range, where the local velocity over the airfoil exceeds sonic speed. Future subsonic aircraft will fly at higher speeds and will more deeply penetrate the supercritical speed range, causing flow separation and a wide range of shocks. The wing pressures for separated flow with shocks are considerably different than those theoretically calculated for attached flow. These differences seriously influence the flutter speed and transient loads.

Discussion

Effects of Supercritical Phenomena on Pressure Distribution

The pressure distribution for steady and unsteady aerodynamics is calculated analytically, using attached flow.[1–13] Both Bergh[4] and Rodden[5] have suggested correction matrices to account for differences in the experimental and analytical values by using a "weighting" matrix to correct the theoretical values. In the supercritical speed range, however, the pressures change so drastically that the kernel function procedures[7–11] are not adequate and the extrapolation and interpolation routines of Bergh[4] and Rodden[5] are not applicable. From a limited amount of data at some mean frequency, Bergh's[4] weighting matrix routine would be a good approximation for all practical frequencies if the flow did not separate. Once separation and shocks occur, no linear methods are available for theoretically predicting the flow accurately; therefore, reliance on the experimental results is necessary.

The supercritical pressure deviations from the theoretical attached flow is dependent on many parameters: the angle of attack; the M-M_{cr}, which is the freestream Mach number minus the critical Mach number; the airfoil shape and thickness; the Reynolds number; the local lift coefficient, which is also related to the local angle of attack; the rigid and elastic angle-of-attack spanwise changes of the wing; the wing sweep; the wing-fuselage-nacelle-pylon interference effects; the reduced frequency; and the amplitude of the disturbance.

The angle of attack and the Mach number perpendicular to the leading edge represent the incoming flow. This flow must expand over the upper surface of the airfoil, reaching its critical Mach number (supersonic locally). Figures 1a and 1b show (from Ref. 12) that the angle of attack increases from 4° in Fig. 1a to 8° in Fig. 1b at Mach 0.59, causing large pressure oscillations between 15 and 45% of chord. These pressure oscillations are due to separation and shock. The effect of Mach number is also shown in Fig. 1c. The pressure traces at 35 and 45% of the chord indicate separation and shock for Mach 0.79 at 4°, while Mach 0.59 shows smooth flow over the entire chord except for some pressure oscillations at the leading edge only. Using a local lift coefficient of 0.49 for 4°,[13] the critical Mach number is approximately 0.41. The $M - M_{cr}$ for the freestream of Mach 0.59 is 0.18. When the freestream value of 0.79 is used, the $M - M_{cr}$ is 0.38. This deeper penetration into the supercritical region causes the separation and shock as shown in Fig. 1c.

The airfoil shape has an important influence on the resulting pressures. The NACA 65 series airfoil, with a maximum thickness between 30–50% of the chord, has been used on current subsonic high-aspect-ratio transports. It should be noted that the maximum thickness occurs between 30–50% of the chord. This is considered a low-drag airfoil. Earlier conventional airfoils, having a maximum thickness at 30% of chord, have the advantage of a reduced separated flow region. From Refs. 14 and 15, much of the aft section of the wing in the area of the aileron has separated flow for the low-drag airfoil, while only a small portion of the wing has separated flow for the conventional airfoil. By the time the flow strikes the aileron, the flow has recovered. The maximum thickness at 50% for the low-drag airfoil and 30% for the conventional airfoil causes the difference. The maximum thickness as far aft as 50% does not have sufficient chord to recover at $M = 0.80$ from the shocks caused by the large pressure peaks.

In full-scale flight where the Reynolds number is higher than the wind tunnel and thus the boundary layer is thicker, the shock occurs further aft and the pressure gradients are pronounced (Figs. 2 and 3). The aft location of the strong shock and the rearward location of the pressure gradients, comparing wind tunnel to flight test for steady-state condi-

Received March 26, 1968; revision received July 1, 1968. This paper has been reduced from the McDonnell Douglas Corporation, Aircraft Division Paper 4659, which acquaints the reader with background information contained in the references and lists the acknowledgments.

* Senior Executive Advisor, Supervisor in Structural Mechanics Section, Douglas Aircraft Division. Member AIAA.

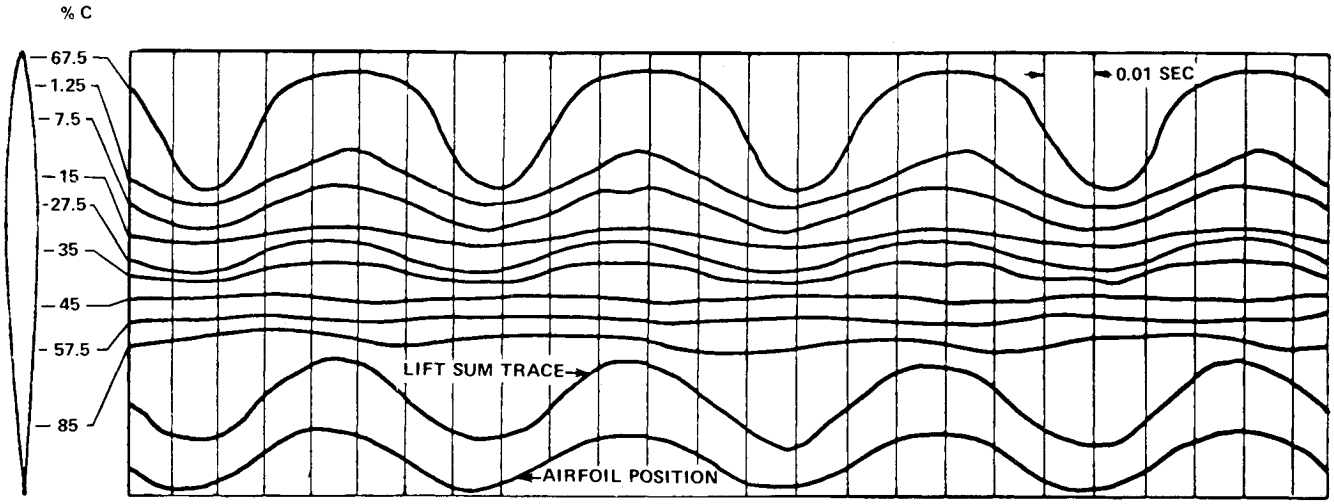

a) 4° MEAN ANGLE OF ATTACK, f = 16.26 CPS, M = 0.59

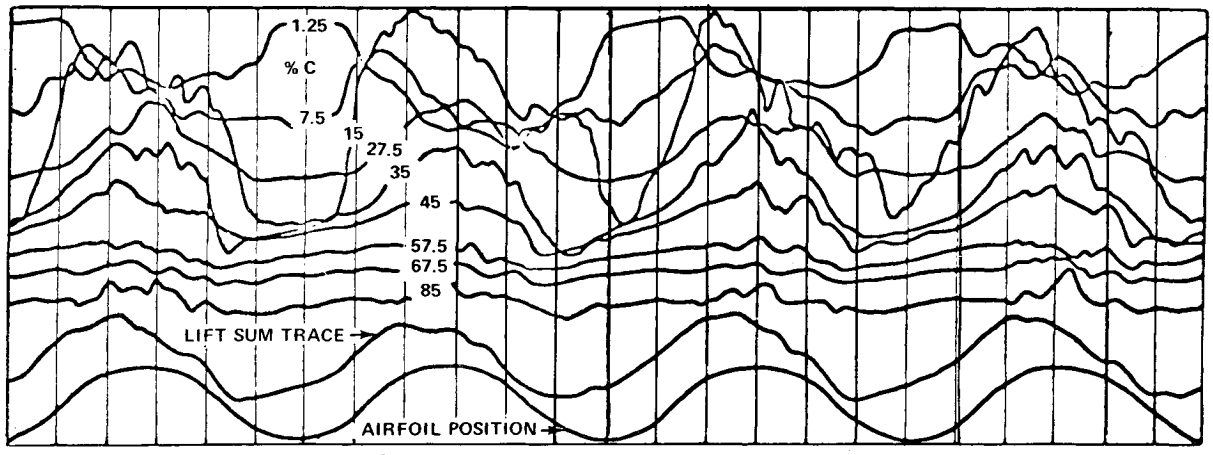

b) 8° MEAN ANGLE OF ATTACK, f = 16.26 CPS, M = 0.59

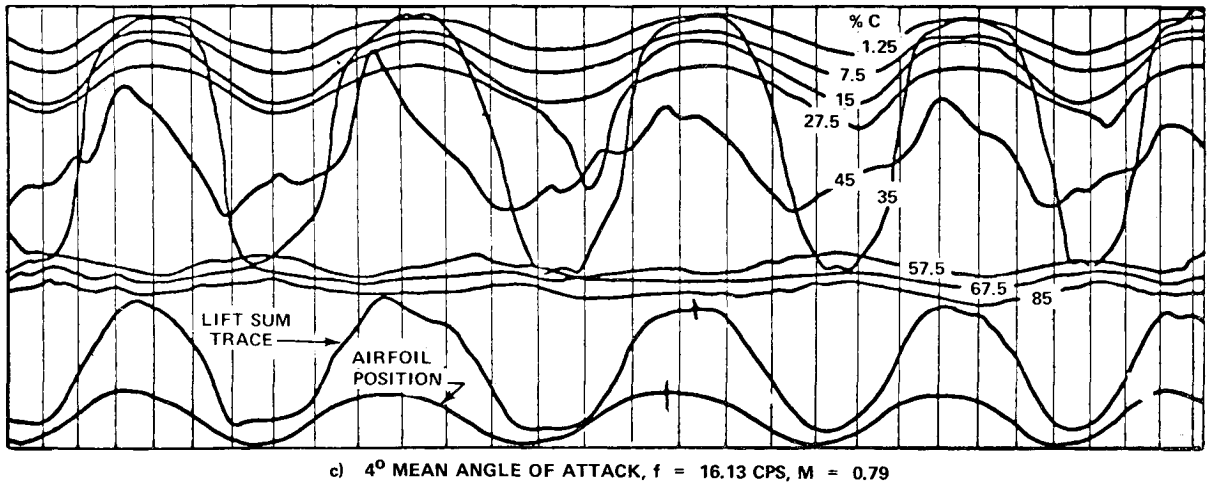

c) 4° MEAN ANGLE OF ATTACK, f = 16.13 CPS, M = 0.79

Fig. 1 Oscillograph records for NACA 65A008 airfoil.

tions, are also expected to influence the unsteady oscillatory coefficients. Figures 4a and 4b show that the strong shock location is influenced by Mach number, aircraft weight, and altitude (W/δ), and Reynolds number of the wind tunnel and flight test. It is necessary to put transition strips on the wind-tunnel model, as described in Ref. 15, to duplicate the flight-test pressure peak position for steady state, $\kappa = 0$, as well as unsteady aerodynamics, $k > 0$. Only if transition strips are used can one expect accurate steady-state and oscillatory coefficients.

Aeroelastic Angles of Attack

The angle of attack of the fuselage reference line was obtained by an aeroelastic analysis. The resulting angle of attack, as a function of the present half span, is shown in Fig. 5 for one particular Mach number based on analysis calculations. A wing-tip vane located on a flight-test tip boom indicated the tip angle shown in Fig. 5. No loads analysis of the tip boom was made to correct for the boom deflection. The tip vane showed a negative angle of attack of −2.5°, while the analysis indicated −2.0. The value of −2.5°

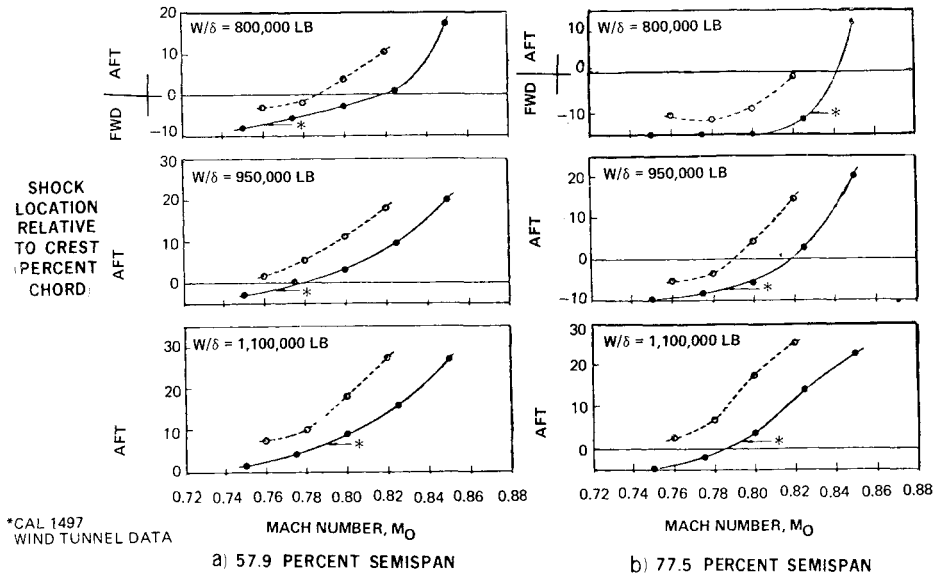

Fig. 2 Strong-shock location on wing upper surface (comparison with wind-tunnel-test results).

was faired into the analysis value for the initial angle of attack for the 1-g condition shown in Fig. 5.

Figure 6 shows the sensitivity of the local slope of the lift curve to the initial 1-g angle of attack. At the critical Mach numbers of 0.85 and 0.875, the local angle-of-attack consideration is important. The angle of attack for zero case is shown for comparison. Cross-plotting some of these data vs Mach number shows the variation of the lift curve slope as a function of Mach number, using the aeroelastic 1-g angles of attack (Fig. 7). The last 40% of the half span is affected by the Mach number.

Compressible Effects of Theoretical Attached Flow Methods on Theodorsen Coefficients

In Ref. 1, Yates obtains an equivalent Fc and Gc using Jordan's theoretical compressibility coefficients. Figure 8 shows how Jordan's coefficients compare to the experimental values. The incompressible Theodoresen values underestimate the phase lag for all Mach numbers. The sonic theory of Nelson and Berman[16] and the theory of Minhinnick[17] show better correlation with experiments at the critical $M = 0.85$ condition.

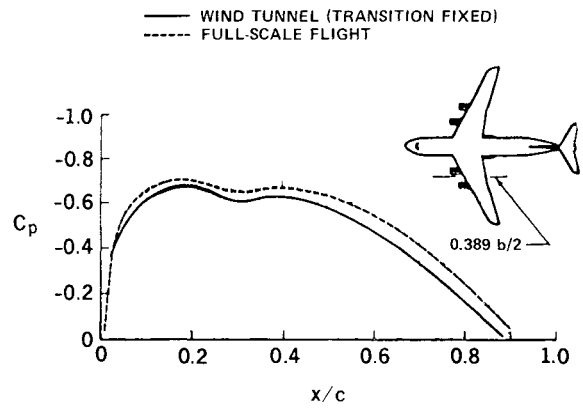

a) 57.9% semispan; M = 0.75, $\alpha_f = -0.6°$

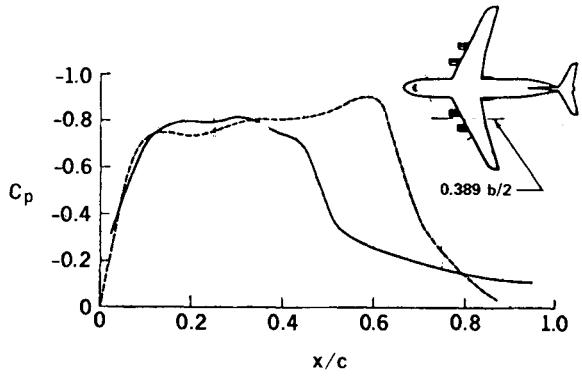

b) 77.5% semispan; M = 0.85, $\alpha_f \approx 0°$

Fig. 3 Subcritical pressure distribution.[15]

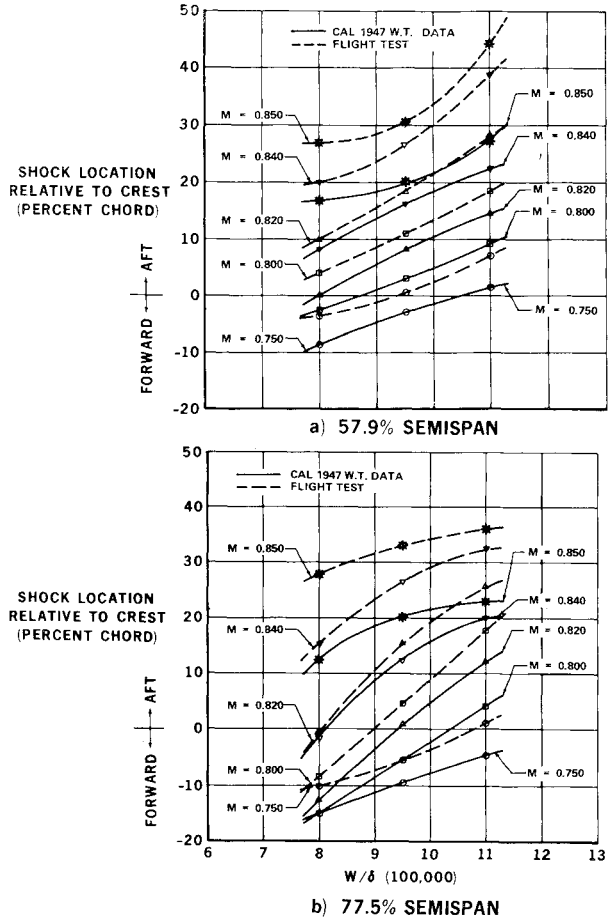

Fig. 4. Strong-shock location on wing upper surface.

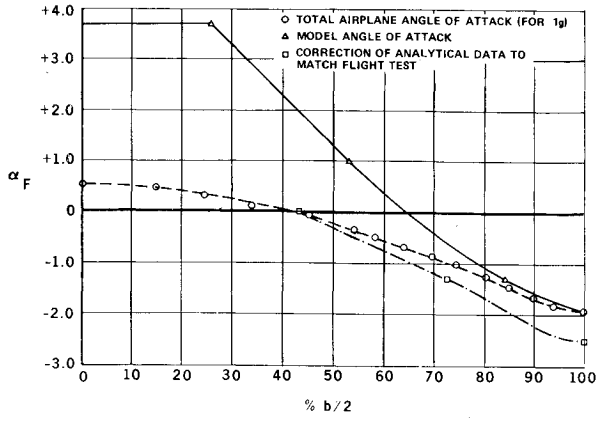

Fig. 5 Aeroelastic angle of attack vs span at 1g (M = 0.85 at 17,500 ft, 100% fuel).

Experimental and Theoretical Flutter Results of $\kappa > 0$

The experimental data obtained were the wing $D_{h\alpha}$ and $D_{\alpha\alpha}$ terms and aileron $D_{\beta\beta}$ terms. Early in the study, large variations in some of the derivatives were used to determine which derivatives were most important. Figure 9 shows how Jordan's coefficients compare to the F and G functions of Theodorsen. Figure 10 shows how the aileron phase angle is affected by the supercritical pressure distribution. The

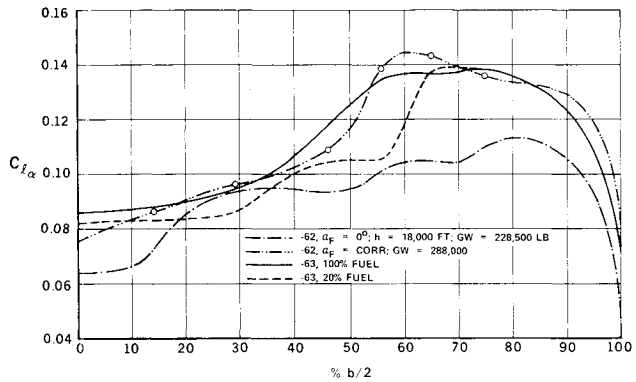

Fig. 6 Wing normal force coefficient curve slope vs $\%b/2$ (due to angle of attack—Mach 0.85).

deeper the penetration ($M - M_{LD}$), the more instability at critical reduced velocities. Values under 180° are unstable; values over 180° are stable. The phase angle is the angle whose tangent is the imaginary to real component. The shock and separation effects on the real component of the aileron-hinge-moment coefficient reduce the wind-tunnel values to very low values over a portion of the wing. Figure 11 shows the effect of reducing these aileron coefficients to 30% of their value. Combining the compressibility effects

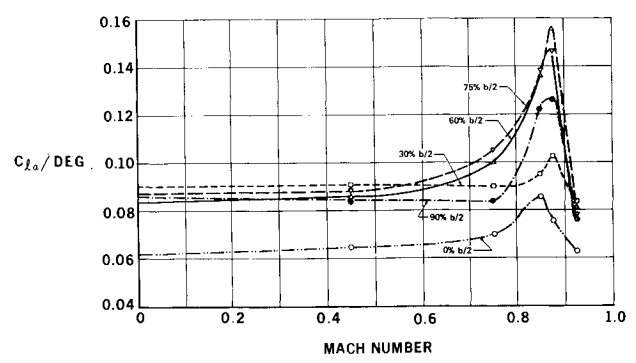

Fig. 7 Wing normal force coefficient lift curve slope vs Mach number (due to angle of attack, 100% fuel, 1g).

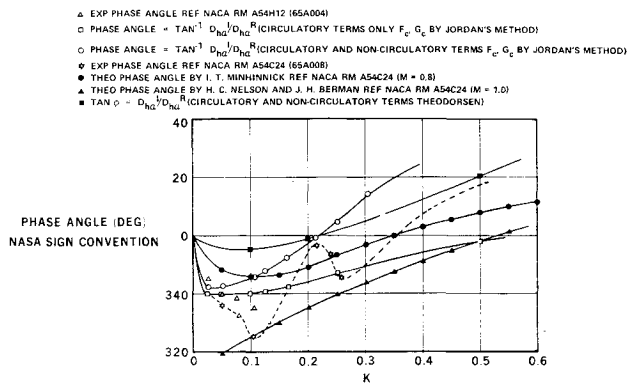

Fig. 8 $D_{h\alpha}$ phase vs theory and experiment (M = 0.85).

of F and G, the real terms for the aileron from flight test, and the phase lag in accordance with Fig. 10, the resulting flutter speeds are shown in Figs. 12 and 13 and are called the J_1 aerodynamics. When the experimental values of the vertical force coefficient phase lag due to angle of attack are added (Fig. 8), the aerodynamics become N_1.

Experimental flight-test information revealed that the J_1 aerodynamics were unconservative, although the N_1 aerodynamics were slightly conservative. The experimental phase angle of pitching moment, taken from Fig. 11 of Ref. 18, was added to the N_1 aerodynamics and is called the N_2

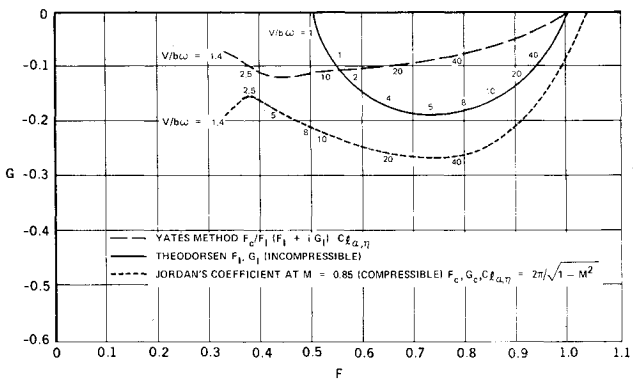

Fig. 9 Comparison of F and G functions for compressible and incompressible flow.

aerodynamics. This effect is much less than the N_1 effect and is shown in Fig. 13. The separated flow effects of the aileron $D_{\beta\beta}$ term, and the wing $D_{h\alpha}$ and $D_{\alpha\alpha}$ terms, are the principal ingredients for reducing the flutter speed at supercritical speeds. Because of the large variation of the $D_{\beta\beta}$ and $D_{h\alpha}$ terms (both real and imaginary), due to angle of attack, Mach number, and Mach critical, the capability of computing the derivatives has been expanded so that it is

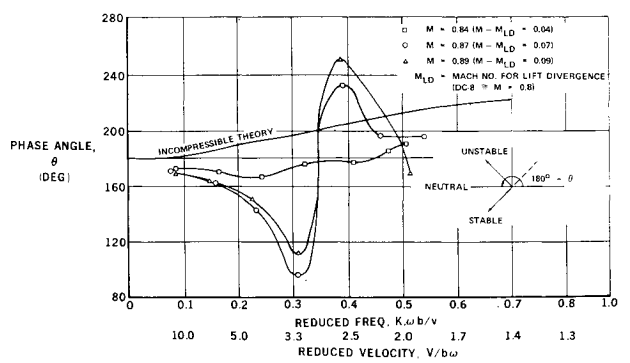

Fig. 10 Theoretical and experimental comparison of aileron phase angle (round nose).

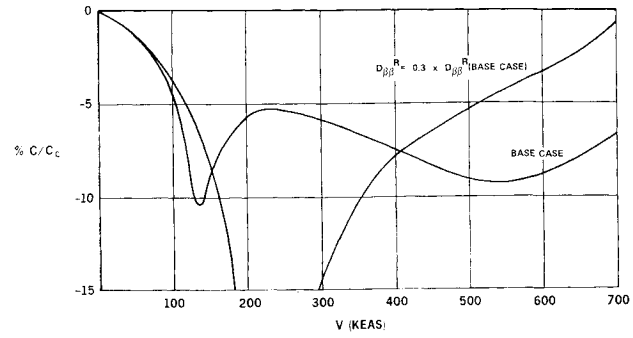

Fig. 11 Effect of aileron-hinge-moment coefficient on flutter speed.

possible to input a derivative as a function of any two of the following variables, varying spanwise (i.e., reduced frequency, κ, Mach number, angle of attack, or $M - M_{cr}$).

Figure 10 shows the phase angle from theory and experiment for an aileron with a round nose. Figure 14 shows the phase angle for an aileron corrected for a 40% nose balance with seals vs reduced frequency and $M - M_{cr}$. Comparing values, the nose balance helps to stabilize the aileron at low supercritical penetration but becomes unstable for deep penetration. These data were input together with the $D_{h\alpha}$ as

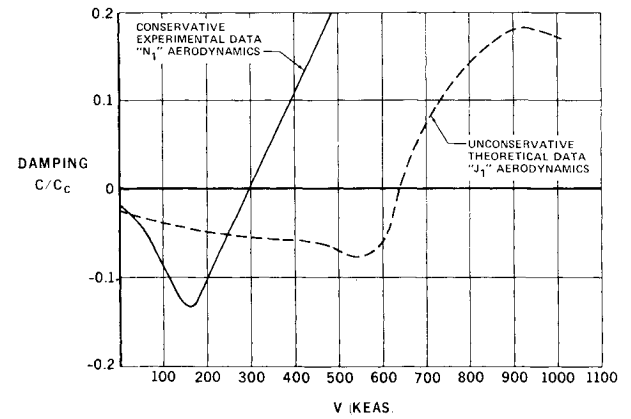

Fig. 12 Effect of aerodynamic theory on flutter speed (M = 0.85 to 0.875).

a function of angle of attack and reduced frequency. Figure 15 shows some of the results of this double interpolation.

The aerodynamic terms were normalized as the reduced velocity was varied and put on polar plots with their phase

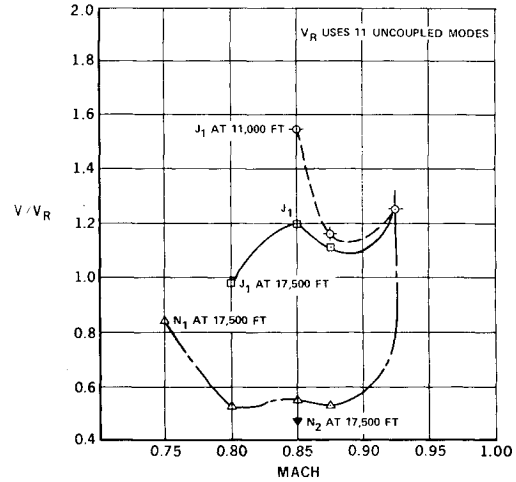

Fig. 13 Flutter speed vs Mach number for J_1 and N_1 aerodynamics.

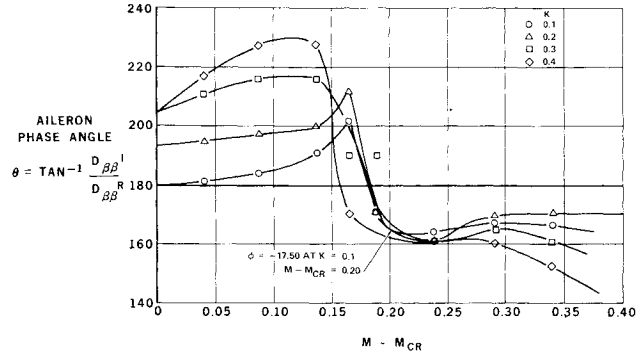

Fig. 14 Phase angle for 30% aileron with 40% C_b/C_F (nose balance).

angles included in order to make comparisons with different aerodynamics. Figure 16 shows the normalized (2π) Theodorsen solution vertical force coefficient due to angle of attack, $N_{h\alpha}$; the normalized vertical force coefficient due to aileron displacement, $N_{h\beta}$; the normalized vertical force coefficient from vertical translation, N_{hh}; the normalized moment term, $N_{\alpha\alpha}$, due to angle of attack; and the normalized moment coefficient due to aileron displacement, $N_{\alpha\beta}$. In Fig. 16, arrows point to the aerodynamic derivative magnitude and

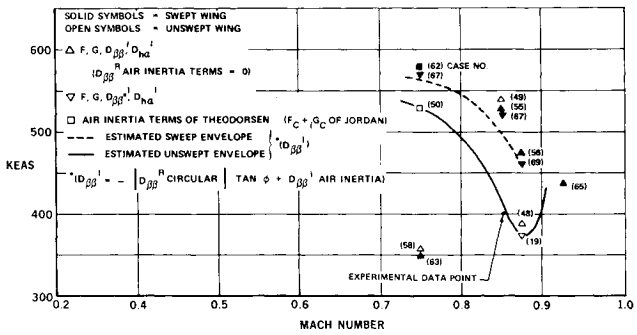

Fig. 15 Flutter velocity vs Mach number using double interpolation for aerodynamics at 17,500 ft ($D^1\beta\beta$ and $D^1h\alpha$ = double interpolation).

phase angle at flutter. The theoretical (2π) analysis of Fig. 16 indicates the following: 1) the $N_{h\alpha}$ term has a lead of 5° and a magnitude of 4.6 for Bay 21, 2) the $N_{h\beta}$ term has a lag of 8° and a magnitude of 3.7, 3) the N_{hh} term has a lag of 7° and a magnitude of 5.6. Figure 17 indicates that an $N_{h\alpha}$ lag of 30° can reduce the flutter speed from 715 to 330 KEAS

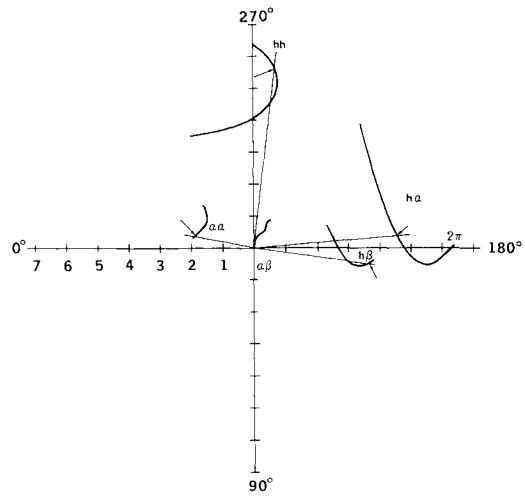

Fig. 16 1B pitch (2π aerodynamics, 715 KEAS, 2.835 cps $v/b\omega$ = 1.35–14.0).

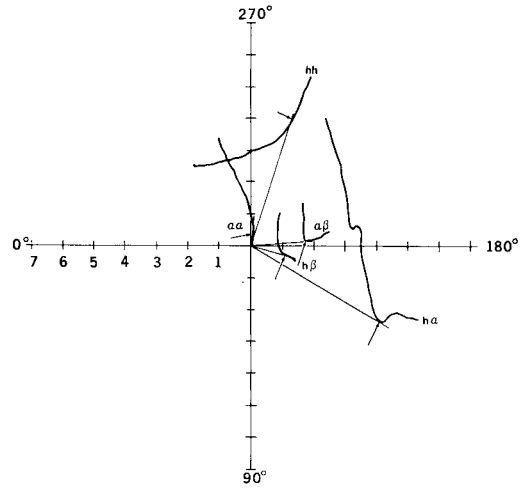

Fig. 17 Wing bending (N_1 aerodynamics, M = 0.85, 330 KEAS, 2.19 cps $v/b\omega$ = 8.0–8.5).

(equivalent air speed in knots). Other parameters are also involved, but essentially, this is the effect of the lag caused by supercritical pressure changes.

When the energy solutions are considered (Figs. 18–20), the damping is the N_{hh} term's vertical component. The vertical force coefficient of the $N_{h\alpha}$ term is usually inputting energy at flutter. The energy from the damping term N_{hh} is very important. As flow separation occurs, the magnitude drops at flutter. Perhaps the most important effect is the lag of the $N_{h\alpha}$ term. The phase angle changes from the lead angle of the Theodorsen (2π) solution to the lag angle of 30° for N_1 at M = 0.85 (Fig. 17), 18° at M − 0.875, and 29° for N_2 at M = 0.85. At flutter, the angle of attack lags the displacement. This modal lag, plus the aerodynamic lag, causes an appreciable vertical component of the $N_{h\alpha}$ term opposing the N_{hh} term. The aileron deflection for the Theodorsen 2π case is close to the 180° phase angle. Including the aerodynamic phase angle of the $N_{h\beta}$ term, the aileron helps to dampen the energy (Fig. 20). For the N_1 aero at M = 0.875, the aileron inputs energy instead of absorbing it (Fig. 18).

The phase angle of the aileron hinge moment is an important parameter. Figure 14 shows that when the Mach penetration into the supercritical range exceeds approximately $M - M_{cr}$ = 0.185, the 40% overbalanced aileron phase angle is unstable for all values of reduced frequency. The round-nosed aileron, on the other hand, is unstable at the low frequencies but stable at the high values of reduced frequency for the supercritical speeds (Fig. 10). Figure 15 shows the effects on flutter speed.

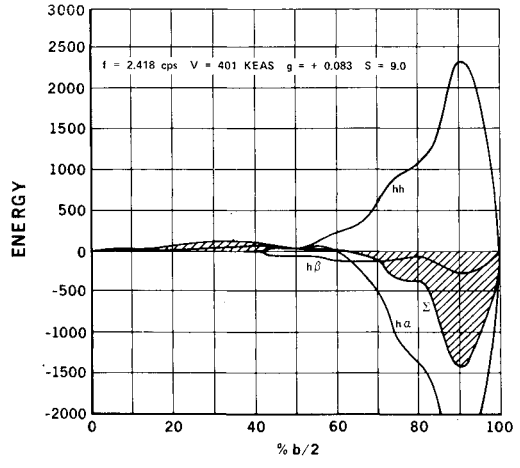

Fig. 18 Energy distribution just past flutter for N_1 aerodynamics at M = 0.875 (mode 1).

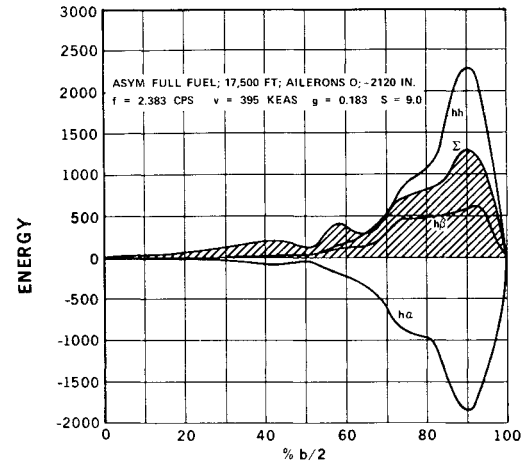

Fig. 19 Energy distribution before flutter for J_1 aerodynamics at M = 0.85, first wing bending (No.1).

The aerodynamic center location was studied. Figure 21 shows that the aerodynamic center location varies with angle of attack from experimental data. The aerodynamic center was obtained from wind-tunnel results using the formula

$$\text{a.c.} = (\text{c.p.} - \text{e.c.}) + \left(\frac{C_l}{dC_l/d\alpha}\right) \times \frac{d\text{c.p.}}{d\alpha}$$

where

a.c.	= aerodynamic center
c.p.	= center of pressure
e.c.	= elastic center
C_l	= local lift coefficient
$dC_l/d\alpha$	= local slope of the lift curve
$d\text{c.p.}/d\alpha$	= rate of change of center of pressure with angle of attack

Figure 15 includes the second term, which reduces the flutter speed. Figure 13 uses only the first term.

The circulatory values of F and G were separated from the total experimental lift and phase angles measured. This was called F_{exp} and G_{exp}. In Fig. 15, the flutter speed has been noted using the experimental values of F and G rather than the theoretical correction due to compressibility suggested by Jordan and called F_c and G_c, which were used for the J_1 values in Fig. 13. Figure 15 includes many other effects. The most important is the inclusion of the vertical force coefficient phase angle and the aileron-hinge-moment phase angle variation spanwise as a function of two variables. The air inertia terms and how they were separated from the circu-

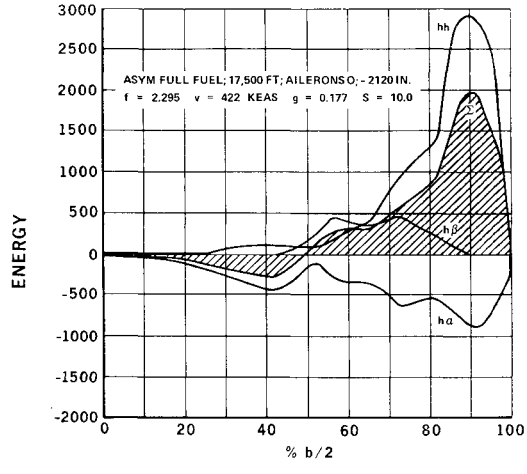

Fig. 20 Energy distribution before flutter for 2π (Theodorsen) aerodynamics—incompressible flow, first wing bending (No. 1).

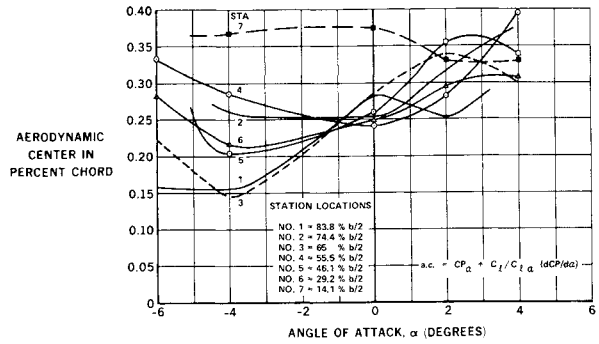

Fig. 21 Wing aerodynamic center vs angle of attack for the DC-8-62 from experimental data (M = 0.875).

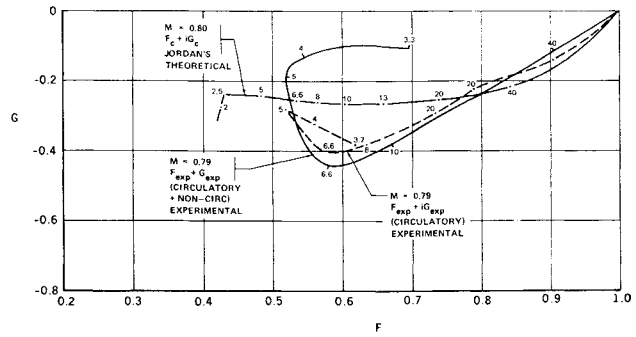

Fig. 22 F and G functions—theoretical and experimental comparison (Jordan at M = 0.80).

latory terms were also found to be important. Using the sweep cosine effect on experimental data for the $D_{h\alpha}$ and $D_{\beta\beta}$ imaginary terms, the F and G functions yield the upper curve shown in Fig. 15.

The lower curve shown in Fig. 15 uses no sweep corrections for $D_{h\alpha}$ and $D_{\beta\beta}$ imaginary terms and yields results closer to the experimental value. Probably, the cosine effect is too large a factor to use when separated flow exists. All the steady-state aerodynamic wind-tunnel data have the sweep effects included. Only the experimental oscillatory coefficients were measured for an unswept wing and need corrections. The sensitivity to the sweep effects indicate that to be slightly conservative, the imaginary terms for $D_{h\alpha}$ and $D_{\beta\beta}$ and Theodorsen F and G should neglect sweep.

Application of Harmonic Wind-Tunnel Results and Theories

Transient dynamic loads and transient flutter analysis can be performed if a realistic approximation for the Wagner indicial lift solution can be substituted in the dynamic equations. By superposition, the Wagner function can represent the circulatory lift for arbitrary motion. Rodden[19] used W. P. Jones'[20] two-term approximation for the exponentials and added an important equation, which represents the lag in the induced aerodynamic loads to the transient aerodynamic influence coefficients matrix equation. Jones' two-term approximation was derived from the general relationship between the coefficients in the exponential approximation and the Theodorsen function, which is

$$1 - \Sigma a_n/(1 - i\beta_n/k) = F(K) + iG(K)$$

[Eq. (10) from Ref. 19].

This is a very important relationship, for it enables one to obtain harmonic aerodynamic data as a function of K and from the experimental F's and G's determine the exponentials used for dynamic transient analysis. The Jones' two-term approximation is for the incompressible Theodorsen coefficients. The analytical Jordan coefficients and the experimental results shown on Fig. 22 were used to obtain the exponential two-term approximations using the equations

$$\beta_1 = \frac{K\left(-G - \dfrac{\alpha_2\beta_2/k}{1 + \beta_2^2/k^2}\right)}{1 - F - \alpha_2/(1 + \beta_2^2/k^2)}$$

and

$$\alpha_1 = \left[\frac{1 + \beta_1^2}{k^2}\right]\left[1 - F - \frac{\alpha_2}{1 + \beta_2^2/k^2}\right]$$

Jones' approximation to Theodorsen's coefficients and the errors vs k are shown in Table 1. Jordan's compressibility coefficient shows F_c and G_c on Fig. 23 for an M = 0.80 case. Table 2 was obtained using the same α_2 and β_2 of Jones and letting close-to-zero error occur in the neighborhood of K = 0.10 where flutter is prevalent. Large errors occur in the low values of K (i.e., at K = 0.25; percent error in F = 8.9; and percent error in G = 19). Most of the effort at this time was to compare the damping between the transient solution and the oscillatory solution. For these flutter solutions, the higher values of K are desired without error.

If the errors in Tables 2 and 3 are not acceptable, new values of β_1 and α_1 must be obtained before the transient analysis proceeds. Further investigation of the experimental results revealed that considerable differences occur in the F and G curves if the noncircular terms are separated from the experimental results. Since the F and G terms are only for the circulatory portion of the lift, the Theodorsen noncirculatory coefficients were separated from the experimental values of $C_{l\alpha}$ to obtain the F value.†

This study shows that flow separation and shock formation in the supercritical range are strong enough to change the oscillatory pressures sufficiently to reduce the flutter speed. The effort in the initial design phases, therefore, should be to consider the following:

1) Use of an airfoil section that can penetrate the supercritical range without strong shocks and flow separation occurring (for example, the NASA Whitcomb wing shape shown in Fig. 24).

Table 1 Theodorsen (using Jones' approximation)[a]

(a) K	(b) $V/b\omega$	(c) F (Theodorsen)	(d) G (Theodorsen)	(e) F (Jones)	(f) F % Error (e)/(c) − 1	(g) G (Jones)	(h) G % Error (g)/(d) − 1
0.4505	2.22	0.377	−0.150	0.613	62.6	−0.173	15.3
0.25	4.0	0.563	−0.185	0.712	26.5	−0.189	2.2
0.1	10.0	0.800	−0.170	0.829	3.6	−0.153	10.0
0.05	20.0	0.902	−0.120	0.893	1.0	−0.132	10.0
0.025	40.0	0.955	−0.0650	0.953	0.21	−0.0993	52.8

[a] Jones' approximation: α_1 = 0.165, β_1 = 0.041, α_2 = 0.355, β_2 = 0.32.

† For an additional list of references relating to many of the subjects of this paper, see Refs. 22–35.

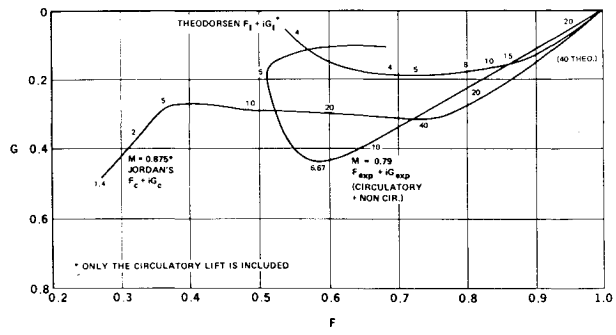

Fig. 23 *F* and *G* functions—theoretical and experimental comparison (Jordan at $M = 0.875$).

2) Use of an airfoil shape with the peak thickness not too far aft. By allowing sufficient chord for pressure recovery, the effects of shocks and separation are minimized.

3) Careful consideration of the effect of the aileron nose balance. A round nose becomes unstable as penetration into the supercritical Mach range exceeds $M - M_{cr}$ of 0.0625. A 40% nose balance delays instability until $M - M_{cr}$ exceeds 0.18. It would seem that keeping a large overbalance would be preferred. The large overbalance, however, drastically reduces the real value of the aileron hinge moment and reduces the flutter speed as shown in Fig. 11. In the area of the nacelle pylons this effect is accentuated, requiring the following compromises:

a) Lock the ailerons or reduce their effective length as the Mach number increases to supercritical speeds. Spoilers can

Table 2 Theoretical compressibility, Jordan at $M - 0.875$[a]

K	$V/b\omega$	F	% e	G	% e
0.4505	2.2	0.213	35.5	−0.208	42.2
0.25	4.0	0.319	8.9	−0.251	19.0
0.1	10.0	0.479	0	−0.290	0
0.05	20.0	0.644	7.3	−0.328	9.3
0.025	40.0	0.837	13.9	−0.281	12.2

[a] Jones' approximation: $\alpha_1 = 0.568$, $\beta_1 = 0.397$, $\alpha_2 = 0.335$, $\beta_2 = 0.022$

be substituted if care is exercised not to make them too effective, causing strength and control problems.

b) Use of more effective aileron dampers with duplication of system for fail-safe conditions.

c) Increase the thickness of the trailing edge of the aileron, which prevents instability and causes the aileron hinge moment to increase.

4) The "energy" solution indicates that the outboard 40% of the wing semispan is critical. Oscillatory tunnel testing using transition strips to push the peak pressure point back to the expected flight-test position is needed. To reduce the peak pressure and therefore the $M - M_{cr}$ penetration, the following can be done:

a) Use a low-wing loading.

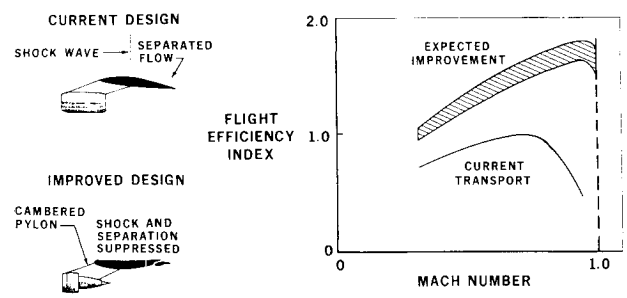

Fig. 24 Subsonic and transonic aerodynamics.

Table 3 Experimental $M = 0.79$, $F_{exp} + iG_{exp}$[a]

K	$V/b\omega$	F	% e	G	% e
0.303	3.3	0.314	54.8	−0.329	213.3
0.25	4.0	0.365	32.8	−0.352	170.8
0.1	10.0	0.660	0	−0.384	0.26
0.05	20.0	0.862	7.8	−0.291	29.3
0.025	40.0	0.959	0.9	−0.170	183.3

[a] Jones' approximation: $\alpha_1 = 0.578$, $\beta_1 = 0.093$, $\alpha = 0.335$, $\beta_2 = 0.32$.

b) Use wing washout since it holds the wing-tip local lift coefficients to lower values, thus preventing supercritical conditions from becoming serious—low values of $M - M_{cr}$.

c) Use sweep. However, the thickening of the boundary-layer outboard, due to spanwise flow with a swept wing, may counter the gain of sweep from local flow perpendicular to the leading edge, causing a lower Mach number than the airplane velocity. This is difficult to evaluate in a wind tunnel because of the Reynolds number effect. A thicker boundary layer, due to flight-test Reynolds number, makes the separation of flow and the shock pressure values greater in magnitude, and moves the shock further aft chordwise. Therefore, the addition of transition strips in the wind tunnel must be included if these effects are to be evaluated. Fences at various spanwise locations, especially near the nacelle-pylon interface protuberances, should be studied carefully to hold the boundary-layer thickness to a minimum and thus take advantage of the wing sweep.

5) New aircraft configuration studies should include the pressures and oscillatory derivatives at high Reynolds numbers, high transonic Mach numbers, and throughout the angle-of-attack range of interest for the new vehicle.

6) The experimental F and G functions shown in Fig. 23 are considerably different than the Theodorsen incompressible flow or the attached flow compressibility effects of Jordan. Therefore, the substitution of the experimental values for the attached flow values of F_c and G_c affect the flutter speed and should be included in any flutter analysis.

7) Unfortunately, the flight test is conducted much later than the wind-tunnel test. Therefore, the chordwise peak pressures are not known when the data are required for design. Therefore, data similar to Figs. 4a and 4b must be relied upon. The aerodynamic data should be obtained with and without transition strips and the airplane designed for both conditions. A worthwhile study by NACA would be to take the models used in Refs. 12 and 22, put on transition strips to duplicate the pressure peak of Ref. 15, and rerun the tests to see what effects the transition strips have on the derivatives when $k > 0$. Only a limited amount of flight-test and wind-tunnel information was available for this study. Future aircraft will require a considerable amount of unsteady aerodynamic tunnel testing and flight correlation if the aircraft is planned to penetrate into the supercritical flight range.

References

[1] Yates, E. C., Jr., "Calculation of Flutter Characteristics for Finite-Span Swept or Unswept Wings at Subsonic and Supersonic Speeds by a Modified Strip Analysis," RML57L10, March 1958, NACA.

[2] Zimmerman, H., "Elementary Static Aerodynamics Adds Significance and Scope in Flutter Analysis," ACR-62, Vol. 1, April 1961, Aerospace Industries Association Office of Naval Research.

[3] Zisfein, B. and Frueh, F. J., "New Dynamic System Concepts and Their Application to Aeroelastic System Approximations," ACR-62, Vol. 1, April 1961, Aerospace Industries Association Office of Naval Research.

[4] Bergh, H. and Zwaan, R. J., "A Method for Estimating Unsteady Pressure Distributions for Arbitrary Vibration Modes from Theory and from Measured Distributions for One Single Mode," NLR-TR F.250, Feb. 1966, National Aerospace Lab., NLR, Amsterdam.

[5] Rodden, W. P. and Revell, J. D., "The Status of Unsteady Aerodynamic Influence Coefficients," Paper FF-33, 1962, IAS/-SMF Fund.

[6] Ashley, H., "Some Recent Developments in Interference Theory for Aeronautical Applications," Rept. 63-3, July 1963, Massachusetts Institute of Technology, Fluid Dynamics Research Lab.

[7] Landahl, M. T., "Kernel Function for Nonplanar Oscillating Surfaces in a Subsonic Flow," *AIAA Journal*, Vol. 5, No. 5, May 1967, pp. 1045–1046.

[8] Andrew, L. V., Vivian, H. T., and Rodemich, E. R., "Unsteady Aerodynamics for Advanced Configurations," FDL-TDR-64-152, Pt. I, Air Force Flight Dynamics Lab.

[9] Rowe, W. S., "Collocation Method for Calculating the Aerodynamic Pressure Distributions on a Lifting Surface Oscillating in Subsonic Compressible Flow," *AIAA Symposium on Structural Dynamics and Aeroelasticity*, AIAA, 1965, pp. 31–45.

[10] Laschka, B., "Zur Theorie Der Harmonisch Schwingenden Fläche Bei Unterschallanströmung," *Zietschrift Fur Flugwissenschaften*, Vol. 11, No. 7, 1963.

[11] Yates, E. C., Jr., "A Kernel-Function Formulation for Nonplanar Lifting Surfaces Oscillating in Subsonic Flow," *AIAA Journal*, Vol. 4, No. 8, Aug. 1966, pp. 1486–1488.

[12] Wyss, J. A. and Herrera, R., "Effects of Angle of Attack and Airfoil Profile on the Two-Dimensional Flutter Derivatives for Airfoils Oscillating in Pitch at High Subsonic Speeds," RM A54H12, Oct. 1954, NACA.

[13] Abbott, I. H., Von Doenhoff, A. E., and Stivers, L. S., Jr., "Summary of Airfoil Data," TR 824, 1945, NACA.

[14] Smilg, B., "The Prevention of Aileron Oscillations at Transonic Airspeeds," AAF TR 5530, Dec. 1946, Air Material Command.

[15] Loving, D. L., "Wind-Tunnel-Flight Correlation of Shock-Induced Separated Flow," TN D-3580, Sept. 1966, NASA.

[16] Nelson, H. C. and Berman, J. H., "Calculations on the Forces and Moments for an Oscillating Wing-Aileron Combination in Two-Dimensional Potential Flow at Sonic Speed," TR 1128, 1953, NACA.

[17] Minhinhick, I. T., "Subsonic Aerodynamic Flutter Derivatives for Wings and Control Surfaces," RAE Structures 87, July 1950, Royal Aeronautical Establishment.

[18] Brown, H. H., Rathert, G. A., Jr., and Clousing, L. A., "Flight-Test Measurements of Aileron Control Surface Behavior at Supercritical Mach Numbers," RN A7A15, April 1947, NACA.

[19] Rodden, W. P., "A Strip Method for Prediction of Damping in Subsonic Flight Flutter Tests," Rept. WPR(DAC) TN-67-1, April 1967, Douglas Aircraft Co. Inc.

[20] Jones, W. P., "Aerodynamic Forces on Wings in Non-Uniform Motion," R & M, 2117, 1945, Aeronautical Research Council.

[21] Fischler, J. E., "Modes of Failure of a Hypersonic Re-Entry Glide Vehicle," *Aerospace Engineering*, Sept. 1961, Vol. 20, No. 9, Part 1, pp. 14–15.

[22] Wyss, J. A. and Monfort, J. C., ' Effects of Airfoil Profile on the Two-Dimensional Flutter Derivatives for Wings Oscillating in Pitch at High Subsonic Speeds," RM A54C24, May 1954, NACA.

[23] Topp, L. J., Rowe, W. S., and Shattuck, A. W., "Aeroelastic Considerations in the Design of Variable Sweep Airplanes," Paper 66-12, Sept. 1966, RAS/ICAS.

[24] Rheinfurth, M. H. and Swift, F. W., "A New Approach to the Explanation of the Flutter Mechanism," *AIAA Symposium on Structural Dynamics and Aeroelasticity*, AIAA, 1965, pp. 1–9.

[25] Stack, J., "Compressible Flows in Aeronautics," *Journal of the Aeronautical Sciences*, Vol. 12, 2, April 1945, Vol. 12, No. 2, pp. 127–148.

[26] Liepman, H. W., "Investigation of the Interaction of Boundary Layer and Shock Waves in Transonic Flow," California Institute of Technology, Supplemental Agreement 4 (S-4843), Contract W33-038 AC-1717 (11592), prepared for the U.S. Army Air Forces, California Institute of Technology, Pasadena, Calif.

[27] Lynch, F. T., "Summary of Results from DC-8 Ship 201 Long-Duct Pod Development Program," Rept. LB 32668, Sept. 1965, Douglas Aircraft Co., Inc.

[28] Levy, L. L., Jr. and Knechtel, E. D., "Experimental Study of the Effects of Sweepback on Transonic Aileron Flutter," RM A51E04, Sept. 1951, NACA.

[29] Jordan, P. F., "Aerodynamic Flutter Coefficients for Subsonic, Sonic and Supersonic Flow (Linear Two-dimensional Theory)," R & M 2932, April 1953.

[30] Erickson, A. L. and Stephenson, J. R., "A Suggested Method of Analyzing for Transonic Flutter of Control Surfaces Based on Available Experimental Evidences," RM A7F30, Dec. 1947, NACA.

[31] Renger, L. H., "Lifting Surface Theory Aerodynamic Influence Coefficients Program Deck Listing and Input Data," Rept. DAC 33847, July 1967, Douglas Aircraft Co., Inc.

[32] Renger, L. H., "Fortran and Quicktran Program for Normalized Lift Coefficient," Rept. DAC 33848, July 1967, Douglas Aircraft Co., Inc.

[33] Fischler, J. E., "Design Considerations for a Supersonic Transport," SAE-ASNE National Aeronautical Meeting Paper 679B, Douglas Paper 1260, April 1963, Douglas Aircraft Co., Inc.

[34] Thomas, B. K., Jr., "New Wing Promises Design Breakthrough," *Aviation Week—Space Technology*, July 1967.

[35] Fischler, J. E., "Methods for Rocket Boosted Aircraft and Missiles," Paper 781, April 1959, Douglas Aircraft Co. Inc.